# Analysis of the ignition dynamics of H 2 -enriched premixed flames using high speed PIV/OH-PLIF

Tarik Yahou, Thierry Schuller, James Dawson

# Analysis of the ignition dynamics of $H_2$-enriched premixed flames using high speed PIV/OH-PLIF

T.Yahou*[1;2], T. Schuller[2], and J. R. Dawson[1]

[1]Department of Energy and Process Engineering NTNU Trondheim, Norway
[2]Institut de Mécanique des Fluides de Toulouse, IMFT Université de Toulouse, CNRS Toulouse, France

**Abstract**

This work combines time-resolved PIV and OH-PLIF to analyze the flame dynamics, from kernel initiation to flame stabilization. Ignition experiments are conducted for increasing hydrogen contents at fixed injection flow velocity $U_b = 5$ m.s$^{-1}$ and constant laminar burning velocity $S_l^0 = 0.25$ m.s$^{-1}$. It was found that the trajectories of the flame leading edge after ignition changes as the $H_2$ content increases. For $CH_4$-air mixtures, the flame is quenched near the injector outlet where the strain rate is high. In this case, the flame cannot penetrate inside the premixed jet exhausting from the burner nozzle and the reactive front is advected downstream along the burner axis. When the hydrogen content increases, stretch resistance grows and the flame front is able to propagate across the outer shear layer near the combustion chamber back plane. This difference between methane and hydrogen flame dynamics is found to be likely the cause of the different types of stabilization modes observed.

## Introduction

Hydrogen is a promising alternative to replace fossil fuels in next generation gas-turbines to achieve a smooth transition towards net zero emissions [1]. Nevertheless, adding increasingly higher amounts of hydrogen to conventional hydrocarbon fuels raises not only important safety concerns from multiple perspectives, but also many challenges that need to be addressed [2]. Due to its high reactivity, $H_2$- enrichment considerably modifies the fundamental combustion process [3], which may compromise compliance with safety standards.

On this matter, one of the major issues driving the design of any aero-engine and/or power plant combustor is to guarantee a safe and reliable ignition sequence for a wide range of $H_2$-content.A successful ignition process is commonly decomposed into a series of successive steps [4]. First, a flame kernel should be initiated by imposing a local energy discharge. This can be achieved using an electric spark plug or a laser [5]. Then comes flame propagation, during which the formed kernel develops to a fully turbulent propagating flame igniting the fresh gases exhausting from the injector nearby. Finally, burner-to-burner flame propagation in multi-injector systems leads to stabilized flames. A large effort has been devoted to the understanding of the mechanisms controlling flame initiation and the determination of minimum ignition energies for various fuels. These studies demonstrated the statistical nature of ignition and its dependence to the local flow properties accounting for complex flow topology as well as its variability during ignition [6]. Recently, research has been concerned with the transition from the initial flame kernel to fully established flames in both single sector [7] and annular combustors with multiple injectors [8]. It has been shown that a successful flame growth is governed by the direction of the instantaneous velocity and the local strain rate in the vicinity of the spark. Recent direct numerical simulations of ignition in high-speed flows above a backward step combustor [9] have shown that the ability of a flame to propagate into different regions of the flow is essentially governed by the local strain rate in the shear regions, leading to flame quenching when the strain rate exceeds a critical extinction threshold.

Due to the high reactivity of hydrogen compared to hydrocarbon fuels, new questions arise for safe ignition of burners powered by hydrogen. Only few studies have been dedicated to assessing the consequences of violent ignition. For instance, due to volumetric expansion of the burned gases, ignition can generate, a strong pressure pulse which may perturb the flow at the injector outlet and lead to flame flashback immediately after ignition of fully premixed systems [10]. Later, Yahou et al. [11, 12] revealed that increasing the hydrogen content in the fuel blend, not only leads to an amplification of the pressure impulse, but also considerably modifies the final stabilization state of the flame. Three different scenarios have been identified: no flashback, transient flashback and permanent flashback. It was also shown that synchronization between this pressure impulse with respect to the maximum of heat release rate leads to preferential conditions to trigger flashback, but no further explanation was provided.

This work combines time-resolved Particle Image Velocimetry (PIV) and OH Planar Laser-Induced Fluorescence (OH-PLIF) to analyze the flame dynamics during the ignition sequence. First, the ignition dynamics of six flames with increasing level of hydrogen content is investigated. This is followed by a detailed analysis of the flame leading edge behavior. Finally, the interaction between the travelling flame branch and the highly strained jet is further scrutinized using synchronized time-resolved PIV/OH-PLIF.

*Corresponding author: tarik.yahou@ntnu.no
Proceedings of the European Combustion Meeting 2023

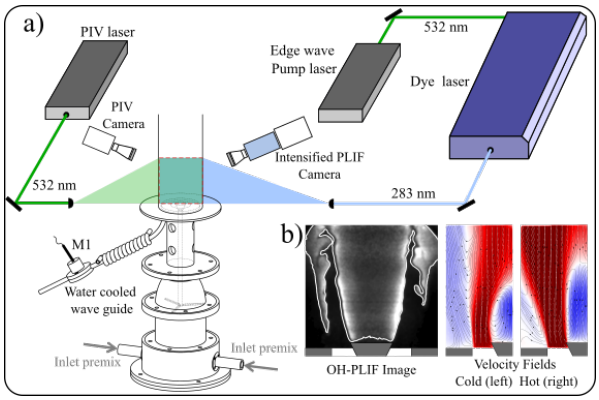


Figure 1: a) Schematic of experimental setup and the laser diagnostic system. b) Example of OH-PLIF image and velocity field from PIV in both cold and hot flow conditions

## Experimental setup and diagnostics

Figure 1.a shows the experimental setup used in this study. The burner consists on a single injector rig operated at atmospheric conditions. A detailed description of the burner geometry is provided in [11]. Ignition experiments are conducted with well premixed $CH_4$-$H_2$ fuels blends. The combustible mixture is supplied through a pipe of 30 mm inner diameter, along which is a 6 mm diameter rod holding a $d_b = 16$ mm conical bluff body, used to stabilize the flame. For optical access purposes, combustion takes place inside a cylindrical quartz chamber of inner diameter $d_{cc} = 60$ mm and total length $l_{cc} = 150$ mm.

The interaction between the flame leading edge and the jet exhausting from the burner is scrutinized combining two-component high-speed OH Planar laser-induced fluorescence (OH-PLIF) system and Particle Image Velocimetry (PIV). The full setup is shown in Fig. 1.a. OH radicals are excited using a 100 W Edgewave green laser (532 nm wavelength) pumping a Sirah Credo-Dye-N laser which, in turn delivers approximately 3 W total output power at 10 kHz. Its wavelength is tuned to match the OH absorption peak near 283 nm. The beam is expanded and collimated into a 1 mm thick laser sheet of total height of 40 mm aligned with the burner axis. A Phantom V2012 high-speed intensified camera, with a gate of 80 ns is used to record flame images. An example of the post-processed PLIF image with the identified flame edge is given in Fig.1.b.

Time-resolved velocity measurements of the flow field during the ignition process are obtained using a high-speed PIV system. The flow is seeded with titanium dioxide particles which are thermally stable up to 2000 K. A 200 mJ dual head Photonics DM100 green laser (532 nm wavelength) is used to illuminate the $TiO_2$ particles, whose beam was shaped into a 1 mm thick light sheet and perfectly aligned with the PLIF system along the central line of the bluff body. Imaging is carried out with a Phantom V2012 camera equipped with a Nikon-Nikkor 200 mm f/2.8 micro lens positioned next to the intensified PLIF camera with 20° angle with respect to normal imaging plane. A Scheimpflug-adapter is used to correct for the plane of focus. To capture the velocity gradients in the shear layer regions, the imaging field-of-view is restricted to half of the combustion chamber $30 \times 50$ mm resulting into 32 pixels/mm spatial resolution. Synchronization of both PLIF and PIV laser pulses and both cameras timing is achieved using a LaVision PTU unit. Images are sampled at $f_s = 10$ kHz with both systems. Vector fields are processed with Davis 8 using a multipass cross correlation algorithm with a final interrogation window of $16 \times 16$ pixels with 50% overlap, resulting in a spatial resolution of 0.25 mm between the computed vectors in both directions. An example of the axial velocity field is given in Fig.1.b for cold and hot flow conditions.

## Operating conditions and ignition procedure

Ignition dynamics is investigated for the full span of $CH_4$/$H_2$ fuel blend, ranging from pure methane (PH0) to pure hydrogen (PH100). The $H_2$-content is increased with step of 20% defined in terms of power fraction $\mathrm{PH} = \mathscr{P}_{H_2} / (\mathscr{P}_{H_2} + \mathscr{P}_{CH_4})$. This study only considers ignition experiments at constant bulk flow velocity $U_b = 5$ m.s$^{-1}$ and fixed laminar burning velocity $S_l^0 = 0.25$ m.s$^{-1}$. In accordance to Tab. 1, the equivalence ratio $\phi$ of the mixture is tuned to maintain a constant burning velocity $S_l^0$. Gases are injected into the bottom plenum at room temperature $T_u = 298$ K.

These operating conditions offer the possibility to partially isolate the flow dynamics from the effects of the combustion properties of hydrogen. Results from [11] have shown that keeping $U_b$ and $S_l^0$ constant effectively scales the response of the pressure time-series. In this way, all levels of PH achieve approximately the same over pressure. For each operating condition, ignition experiments are repeated eight to ten times to verify the repeatability of each sequence and allow accurate statistical measurements.

To initiate the first flame kernel, an electric spark plug connected to a Danfoss EB14 transformer is used to deliver 36 mJ mean energy at a rate of $f_s = 50$ Hz. Each spark lasts 7.5 ms. The igniter is positioned in the outer recirculation zone above the combustor back plate, approximately 20 mm away from the center of the bluff-body. To minimize wall temperature effects on the ignition dynamics [13], care is taken to maintain constant thermal conditions by following a strict exper-

Table 1: Operating conditions at $U_b = 5$ m.s$^{-1}$ and $S_l^0 = 0.25$ m.s$^{-1}$ for six different levels of $H_2$-enrichment.

| Cases | $\phi$ | $\mathscr{P}_{CH_4}$ | $\mathscr{P}_{H_2}$ | $T_{ad}$ [K] | $\mathscr{P}$ [kW] |
|---|---|---|---|---|---|
| PH0 | 0.78 | 100% | 0% | 1980 | 8.4 |
| PH20 | 0.68 | 80% | 20% | 1850 | 7.6 |
| PH40 | 0.60 | 60% | 40% | 1740 | 6.9 |
| PH60 | 0.53 | 40% | 60% | 1630 | 6.3 |
| PH80 | 0.48 | 20% | 80% | 1580 | 6.0 |
| PH100 | 0.43 | 0% | 100% | 1500 | 5.7 |

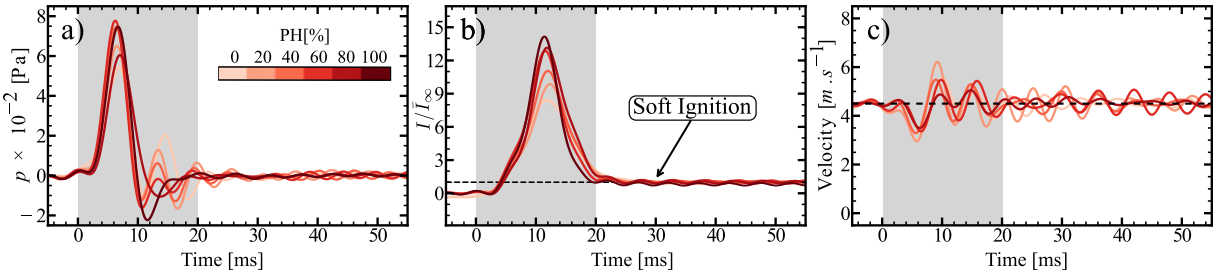


Figure 2: Time traces, averaged over ten runs, of chamber pressure (a), normalized OH* light intensity (b) and injector flow velocity (b) for the six different flames presented in Tab. 1. The gray zone denotes the transient perturbation.

imental procedure: (i) The burner is first preheated up to a temperature 470 K measured at the center of the bluff-body using a pyrometer. (ii) The chamber is then filled with the combustible mixture for 5 s to ensure ignition occurs in a homogeneous fuel air mixture. (iii) Five successive sparks corresponding to a sparking time window of 100 ms are produced. In the event of an ignition failure within this time interval, the ignition sequence is stopped, the combustion chamber is purged and the procedure is restarted again.

**Ignition dynamics**

Before scrutinizing the interaction between the flame leading edge and the jet flowing out of the burner during the ignition process, the transient response of the flow is first analyzed for operating conditions defined in Tab. 1. Time-resolved chamber pressure, OH* chemiluminescence and injector flow velocity are recorded simultaneously using, a microphone labelled M1 in Fig. 1, a photomultiplier equipped with an OH* filter and a hot wire (HW) probe, respectively. The velocity is measured 70 mm upstream of the injector lips.

Figure 2.a-c plots their time-series averaged over ten runs. The instant, $t = 0$ ms, marks the formation of the first flame kernel detected by the photomultiplier module. Consistently with previous work [11], the response pressure inside the combustion chamber scales with constant $U_b$ and $S_l^0$. All the flames, regardless the $H_2$-content in the mixture, achieve approximately the same pressure peak around 700 Pa (Fig. 2.a). For these atmospheric conditions i.e., the chamber back pressure is nearly zero, the combustion products can freely expand as there is no flow restriction at the outlet of the combustion chamber. Therefore, this leads to a soft ignition scenario for the full span of $H_2$-content, where all the six flames directly stabilize after ignition as seen in Fig. 2.b.

The pressure overshoot is in these cases not sufficient to significantly modify the flow velocity inside the injector. Figure 2.c confirms that the injector flowrate only slightly decreases as the chamber pressure rises. The flow velocity through the injector is only reduced down to 3.5 m.s$^{-1}$ around $t = 6$ ms after ignition. This approximately matches the instant when the pressure reaches its maximum in Fig. 2.a. In this case, the ratio of the bulk flow velocity to the laminar burning velocity remains high enough $\left(U_b/S_l^0\right)_{min} \simeq 14$ to prevent flashback after ignition.

Although no flashback is observed with the selected configuration, analyzing the flame leading edge behavior during ignition, is useful to understand the flashback mechanism when triggered by ignition dynamics. As a consequence of the relatively weak velocity perturbation, the flow field at the first instants of the ignition sequence can be assumed close to the mean steady field before ignition.

**Flame leading edge behavior**

In this section, OH-PLIF is used to analyze the flame dynamics, from kernel formation to final stabilization. Experiments are performed for three specific operating conditions with increasing $H_2$-contents corresponding to PH0, PH40 and PH100 flames (see Tab. 1). It was shown in Yahou et al. [11] that these flames lead to a three different ignition scenarios: a soft ignition scenario for PH0, a transient and permanent flashback scenario for PH40 and PH100, respectively. The aim here is to investigate the impact of the hydrogen enrichment on the flame leading edge dynamics during the ignition sequence.

Figure 3 shows six successive snapshots of OH-PLIF along the central plane. For PH0 flame (top row), experiments reveal that during the first instants of the ignition sequence, the flame is quenched near the outer shear layer of the jet where high flow stress is expected. In this case, the flame leading edge cannot penetrate inside the premixed jet exhausting from the burner nozzle and the reactive front is advected away in the vertical direction. As the flame propagates further downstream, the strain rate decreases and the leading point penetrates within the central jet at a distance $d_p = 25$ mm from the chamber back plane (see snapshot at $t = 10$ ms). The same leading point follows its path and propagate towards the bluff-body igniting the entire central recirculation zone from the top. This is followed by a smooth consumption of all the fresh gases until full ignition and final stabilization.

As the $H_2$-content in fuel blend increases, the flame leading point penetrates through the outer shear layer of the jet at smaller distances $d_p$ with respect to the chamber back plane. In these new conditions, OH-PLIF images in Fig. 3 show that the penetration distance $d_p$

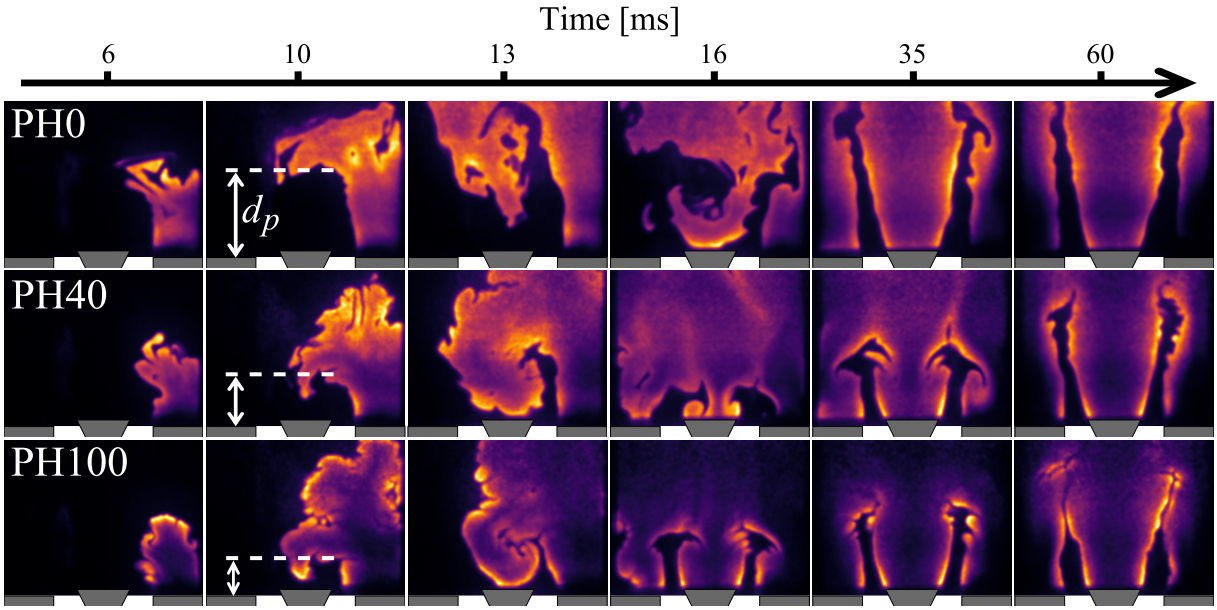


Figure 3: Instantaneous OH-PLIF snapshots showing the ignition sequence along the central plane from kernel formation to final stabilization for PH0 (top row), PH40 (mid-row) and PH100 (bottom figure).

decreases down to 15 mm and 10 mm for PH40 and PH100, respectively. For both mixtures, the flame leading edge propagation is barely affected by the high flow stress in the vicinity of the injector lips, igniting the whole chamber until stabilization.

**Flow field analysis**

To further assess the observed differences in terms of leading point behavior, it is interesting to consider the extinction strain rate $\kappa_{ext}$ of each flames reported in Tab. 1. To do so, the consumption speed $S_c$ normalized by the laminar unstrained burning velocity $S_l^0$ is calculated for increasing global strain rates $\kappa_s = \Delta U/\Delta x$. The simulations are performed at atmospheric conditions at $T_u = 300$ K using the 1D twin premixed flames configuration from Cantera and the results are plotted in Fig. 4. The consumption speed is deduced from [14]:

$$S_c = -\frac{1}{\rho_u Y_F^u}\int_{-\infty}^{+\infty} \dot{\omega} d\mathbf{n} \qquad (1)$$

In accordance with theory, the $CH_4$-Air flame ($Le \simeq 1$) at $\phi = 0.78$ remains insensitive to stretch and its extinction strain rate is found to be $\kappa_{ext} \simeq 900$ s$^{-1}$ (light red curve in Fig. 4). When the $H_2$-content increases, although the laminar burning velocity is kept constant, the resistance to stretch grows up to $\kappa_{ext} \simeq 1950$ s$^{-1}$ and $\kappa_{ext} \simeq 3200$ s$^{-1}$ for PH40 and PH100, respectively.

To gain a better understanding of the flame leading edge dynamics, it is important to analyze the non-reacting flow field prior to ignition. Figure 5 shows the axial $U_z$ and the tangential $U_x$ velocities as well as the longitudinal strain rate $\kappa_s = \Delta U_z/\Delta_x$ before the onset of combustion. Notably, similar measurements are taken across the six different mixtures outlined in Tab. 1, and the results are consistent. Experiments show that the combustible mixture is injected into the chamber at $u \simeq 8$ m.s$^{-1}$ at the nozzle before the full expansion of the jet further downstream. Close to the spark plug ($r = 20$ mm), both axial and tangential velocities are nearly zero ($U_z = 0.5$ and $U_x = 0.3$ m.s$^{-1}$), indicating that the initial flame kernel freely propagates in a quasi-stagnant flow during the first instants of the ignition sequence.

Interestingly, flow fields reveal that the central recirculation zone produced by the annular jet features a total height of 23 mm above the bluff body. This height approximately corresponds to the penetration distance $d_p = 25$ mm of the $CH_4$-Air flame, as shown in Fig.3. Up to this location, the strain rate in the mixing layer

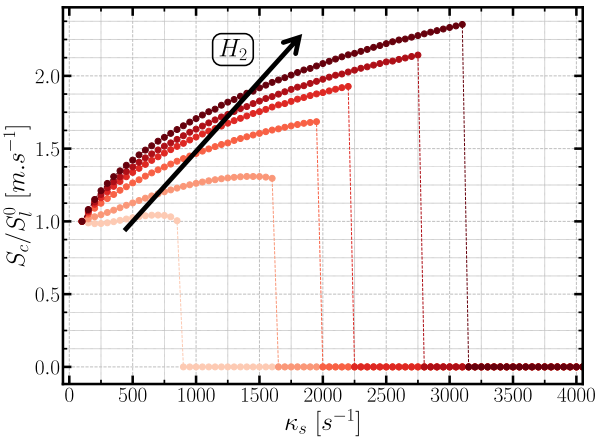


Figure 4: Normalized flame consumption speed highlighting the extinction strain rate of flames presented in Tab. 1. Simulations are performed using the twin premixed flames configuration from Cantera with GRI-Mech 3.0 at 300 K and 1 atm. For the color legends, refer to Fig. 2.

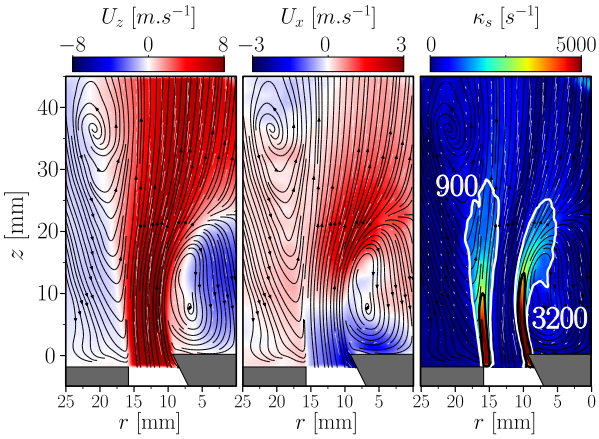


Figure 5: Time-averaged axial $U_z$ and tangential $U_x$ velocities and longitudinal strain rate $\kappa_s$ fields. White and gray iso-contours denote the extinction strain rate $\kappa_{ext}$ of the PH0 and PH100 flames, respectively.

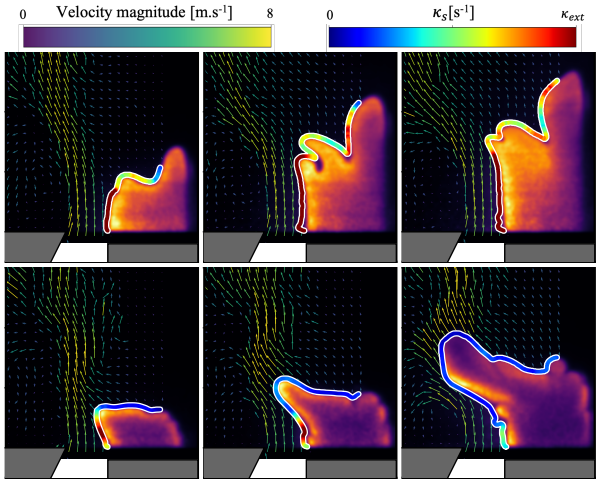


Figure 6: Combined OH-PLIF - PIV data recorded simultaneously during ignition of the $CH4_4$-Air (top row) and $H_2$-Air (bottom row) flames in Tab. 1. For clarity, only $1/5$ velocity vectors are plotted and colored by their magnitude and the flame edge by the local strain rate.

exceeds the critical extinction strain rate $\kappa_{ext} = 900$ s$^{-1}$ (white iso-contours in Fig. 5), preventing the flame from propagating inside the jet. In this case, the flame is constrained to propagate axially along the outer recirculation zone, where the local strain rate remains below $\kappa_{ext}$. This comes to explain the behavior of the PH0 flame: the reaction can only be sustained in some specific regions outside the white iso-contours. Therefore, forcing the reacting front to go all around the jet, before finally entering the central recirculation zone from the top where $\kappa_s \ll \kappa_{ext}$.

Similarly, the black iso-contours denotes the critical extinction strain rate of the $H_2$-Air flames (PH100) $\kappa_s = 3200$ s$^{-1}$. Again, its height $\sim 10$ mm is in excellent correspondence with the penetration distance $d_p = 10$ mm, previously observed in Fig. 3. In this case, the reaction can be sustained in higher flow stress regions and the leading edge is able to propagate through the mixing layer of the jet, quickly reaching the central recirculation zone.

**Flame-jet interactions**

As noted previously in this study, the leading edge behavior during the ignition sequence is highly affected by the local strain rate of the flow. Instantaneously, the global flow varies as the reaction front propagates inside the chamber. It is therefore interesting to scrutinize its interaction with the mixing layer of the jet. This is done by combining time-resolved OH-PLIF and PIV measurements recorded simultaneously. Figure 6 shows the instantaneous reaction front plotted on top of its corresponding velocity field for PH0 (top row) and PH100 (bottom row). This figure clearly shows that for PH0 case, the reaction fronts in contact with the jet are subjected to a very high stretch exceeding the flame quenching limit $\kappa_{ext}$ as highlighted in red along the flame front. On the other hand, the flame edge inside the outer recirculation zone features a strain rate $\kappa_s < \kappa_{ext}$, allowing both the existence and the propagation of the reaction front in this zone. Except for the close vicinity of the nozzle, this is not observed for the PH100 flame, in which case almost the entire leading edge features a strain rate lower than the extinction threshold $\kappa_{ext} = 3200$ s$^{-1}$. In this case the flame propagation is not blocked, and its leading point is able to penetrate through the mixing layer and quickly propagate towards the bluff-body.

This is best seen in Fig. 7 where the probability density function (pdf) of the longitudinal strain rate $\kappa_s$ along the flame front is plotted. For the sake of brevity, anal-

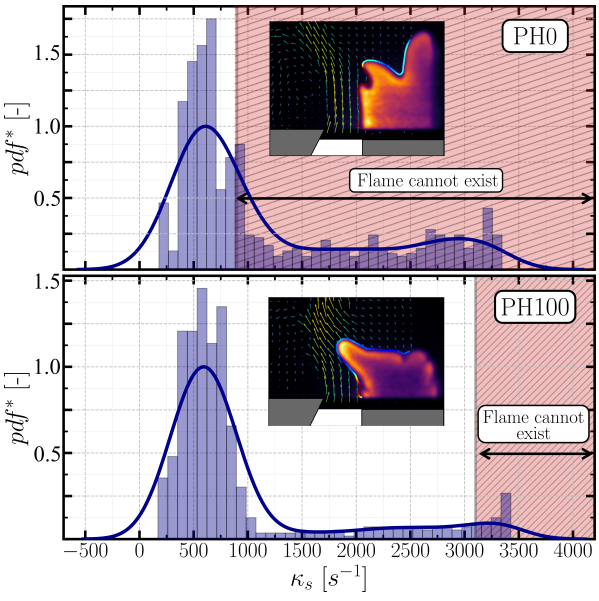


Figure 7: Normalized pdf of the strain rate $\kappa_s$ as well as its corresponding histogram along the flame front for PH0 and PH100 flames. The red hatched part represents the strain rate values above the extinction limit $\kappa_{ext}$.

ysis only considers a single snapshot for both PH0 and PH100. It shows that for $CH_4$-flames, the majority of the flamelet elements is subjected to a strain rate exceeding the extinction limit ($\kappa_s > \kappa_{ext} = 900\ s^{-1}$) highlighted by the red hashed zone, where the reaction cannot be sustained anymore. Conversely, the pdf of $H_2$-Air flame peaks at $\kappa_s \sim 600\ s^{-1}$ which is almost an order magnitude lower than the quenching limit at $3200\ s^{-1}$.

## Conclusion

This paper combines the time-resolved OH-PLIF/PIV diagnostics to analyze the flame leading edge dynamics of $CH_4$-$H_2$-Air flames. For all the fuel blends, the bulk flow velocity was maintained constant at $U_b = 5\ m.s^{-1}$. The hydrogen enrichment was achieved by keeping a fixed value of laminar burning velocity at $S_l^0 = 0.25\ m.s^{-1}$.

The trajectory of the flame leading edge after ignition showed a strong dependence on the $H_2$-content in the fuel bled. For $CH_4$-Air mixtures, it was observed that the flamelet elements in the vicinity of the outer shear layer of the jet are subjected to a high strain rate exceeding the extinction limit. In this zone, the reaction cannot be sustained and the reactive front is advected vertically away from the bunrer back plate, before igniting the central recirculation zone from its top. The flame penetration distance was found to be approximately similar to the height of the central recirculation zone at $d_p = 25$ mm.

When the hydrogen content increases, flame resistance to stretch grows and the flame leading point is able to penetrate through the jet mixing layer at distances closer to the chamber back plane at $d_p = 15$ mm and $d_p = 10$ mm for PH40 and PH100, respectively. Due to its high resistance to stretch, the majority of the flamelet elements features a strain rate lower than the extinction limit, offering favorable conditions for the flame growth.

This difference between methane and $H_2$-enriched flames are likely considered to be the cause of the different stabilization modes observed in Yahou et al. [11]. In the case of the non-penetration due to high strain rate in mixing layer, the flame propagation is temporary slowed down as the leading edge is constrained to propagate axially until a region where $\kappa_s < \kappa_{ext}$. This helps to keep the flame away from the injector when the injection speed decreases due to the ignition over-pressure inside the combustion chamber. Conversely, a quicker penetration of the flame leading edge offers preferential conditions to get the reaction front in the vicinity of the injector when the injection velocity drops, which can be favorable to flashback.

## Acknowledgments

The authors acknowledge support from the NCCS Centre, funded under the Norwegian research program, Centres for Environment-friendly Energy Research (FME) (Grant 257579/E20). Eirik Æsøy is also highly acknowledged for providing insight and expertise on PLIF lasers.

## References

[1] T. Capurso, M. Stefanizzi, M. Torresi, and S. M. Camporeale, Perspective of the role of hydrogen in the 21st century energy transition, *Energy Convers. Manag.* **251**, 114898 (2022).

[2] M. R. Bothien, A. Ciani, J. P. Wood, and G. Fruechtel, Toward decarbonized power generation with gas turbines by using sequential combustion for burning hydrogen, *J. Eng. Gas Turbines Power* **141**, 121013 (2019).

[3] A. L. Sánchez and F. A. Williams, Recent advances in understanding of flammability characteristics of hydrogen, *Prog. Energy Combust. Sci.* **41**, 1 (2014).

[4] A. H. Lefebvre and D. R. Ballal, *Gas turbine combustion: alternative fuels and emissions* (CRC press, 2010).

[5] R. Maly and M. Vogel, in *Symposium (international) on combustion* (Elsevier, 1979), vol. 17, 821–831.

[6] E. Mastorakos, Ignition of turbulent non-premixed flames, *Prog. Energy Combust. Sci.* **35**, 57 (2009).

[7] M. Cordier, A. Vandel, G. Cabot, B. Renou, and A. M. Boukhalfa, Laser-induced spark ignition of premixed confined swirled flames, *Combust. Sci. Technol.* **185**, 379 (2013).

[8] J.-F. Bourgouin, D. Durox, T. Schuller, J. Beaunier, and S. Candel, Ignition dynamics of an annular combustor equipped with multiple swirling injectors, *Combust. Flame* **160**, 1398 (2013).

[9] P. Pouech, F. Duchaine, and T. Poinsot, Premixed flame ignition in high-speed flows over a backward facing step, *Combust. Flame* **229**, 111398 (2021).

[10] K. Prieur, G. Vignat, D. Durox, T. Schuller, and S. Candel, Flame and spray dynamics during the light-round process in an annular system equipped with multiple swirl spray injectors, *J. Eng. Gas Turbines Power* **141** (2019).

[11] T. Yahou, J. R. Dawson, and T. Schuller, Impact of chamber back pressure on the ignition dynamics of hydrogen enriched premixed flames, *Proc. Combust. Inst.* (2022).

[12] T. Yahou, T. Schuller, and J. R. Dawson, The Effect of Ignition Procedure on Flashback of Hydrogen-Enriched Flames, *J. Eng. Gas Turbines Power* **146**, 11021 (2024).

[13] S. Puggelli, T. Lancien, K. Prieur, D. Durox, S. Candel, and R. Vicquelin, Impact of wall temperature in large eddy simulation of light-round in an annular liquid fueled combustor and assessment of wall models, *Journal of Engineering for Gas Turbines and Power* **142** (2020).

[14] T. Poinsot and D. Veynante, *Theoretical and numerical combustion* (RT Edwards, Inc., 2005).